Supplement for
Horizontal redistribution of orographic gravity wave flux in a global chemistry-climate model

Roland Eichinger[1,2], Sebastian Rhode[3], Hella Garny[2,4], Peter Preusse[3], Petr Pisoft[2], Aleš Kuchař[5], Patrick Jöckel[1], Astrid Kerkweg[6], and Bastian Kern[1]

[1]Deutsches Zentrum für Luft- und Raumfahrt (DLR), Institut für Physik der Atmosphäre, Oberpfaffenhofen, Germany
[2]Charles University Prague, Faculty of Mathematics and Physics, Department of Atmospheric Physics, Prague, Czech Republic
[3]Forschungszentrum Jülich GmbH, Institut für Energie- und Klimaforschung, IEK-7, Jülich, Germany
[4]Ludwig-Maximilians-University Munich, Meteorological Institute, Munich, Germany
[5]Universität Leipzig, Institute for Meteorology, Leipzig, Germany
[6]Forschungszentrum Jülich GmbH, Institut für Energie- und Klimaforschung, IEK-8, Jülich, Germany

Correspondence: R. Eichinger (roland.eichinger@dlr.de)

S1 Additional information on the subgrid-scale orography updates

As stated in the main text, the updated parameters for the subgrid-scale orography (SSO) for mean, standard deviation, as well as peaks (maximum) and valleys (minimum) are computed directly from the ETOPO1 data set (Amante and Eakins, 2009) within the corresponding model grid cells (T42). The latter three of these parameters are shown in Fig. S1 in comparison to the standard EMAC SSO, exemplarily for the region around Patagonia and the Antarctic Peninsula.

The other three required parameters, namely anisotropy, slope and main orographic angle, are derived from the former ones by using the equations described by Lott and Miller (1997) and by Baines and Palmer (1990), which are here briefly recapitulated.

With

$$K = \frac{1}{2} \cdot \left[\overline{\left(\frac{\partial h}{\partial x}\right)^2} + \overline{\left(\frac{\partial h}{\partial y}\right)^2} \right], \quad L = \frac{1}{2} \cdot \left[\overline{\left(\frac{\partial h}{\partial x}\right)^2} - \overline{\left(\frac{\partial h}{\partial y}\right)^2} \right], \quad M = \overline{\frac{\partial h}{\partial x} \cdot \frac{\partial h}{\partial y}}, \tag{S1}$$

where h is the mean SSO and the overline corresponds to the mean over the whole grid cell of the corresponding quantity, the main orographic angle can be determined by

$$\theta = \frac{1}{2} \cdot \arctan\left(\frac{M}{L}\right). \tag{S2}$$

This denotes the direction with the largest gradient of topographic variations. The corresponding minimum variation is perpendicular. Changing coordinates to x' and y' which are oriented along the principal axes, K, L and M relative to these axes (K', L' and M') are

$$K' = K, \quad L' = \sqrt{L^2 + M^2}, \quad M' = 0 \tag{S3}$$

With this, the anisotropy of the orography, or 'aspect ratio' can be defined by

$$\gamma = \frac{\overline{\left(\frac{\partial h}{\partial y'}\right)^2}}{\overline{\left(\frac{\partial h}{\partial x'}\right)^2}} = \frac{K' - L'}{K' + L'} = \frac{K - \sqrt{L^2 + M^2}}{K + \sqrt{L^2 + M^2}}. \tag{S4}$$

If the low-level wind vector is directed at an angle φ relative to the x-axis, then the angle between the wind and the mountain's primary axis, ψ, is given by

$$\psi = \theta - \varphi \tag{S5}$$

The slope parameter σ, is defined as

$$\sigma^2 = \overline{\left(\frac{\partial h}{\partial x'}\right)}, \tag{S6}$$

i.e. the mean-square gradient along the principal axis.

For the update, we use the high resolution 1' $\times$ 1' ETOPO1 data in the same manner. Exemplarily, Fig. S2 shows the main orographic angle, anisotopy, and slope of the standard SSO and of the updated version for southern South America and the Antarctic Pensinsula.

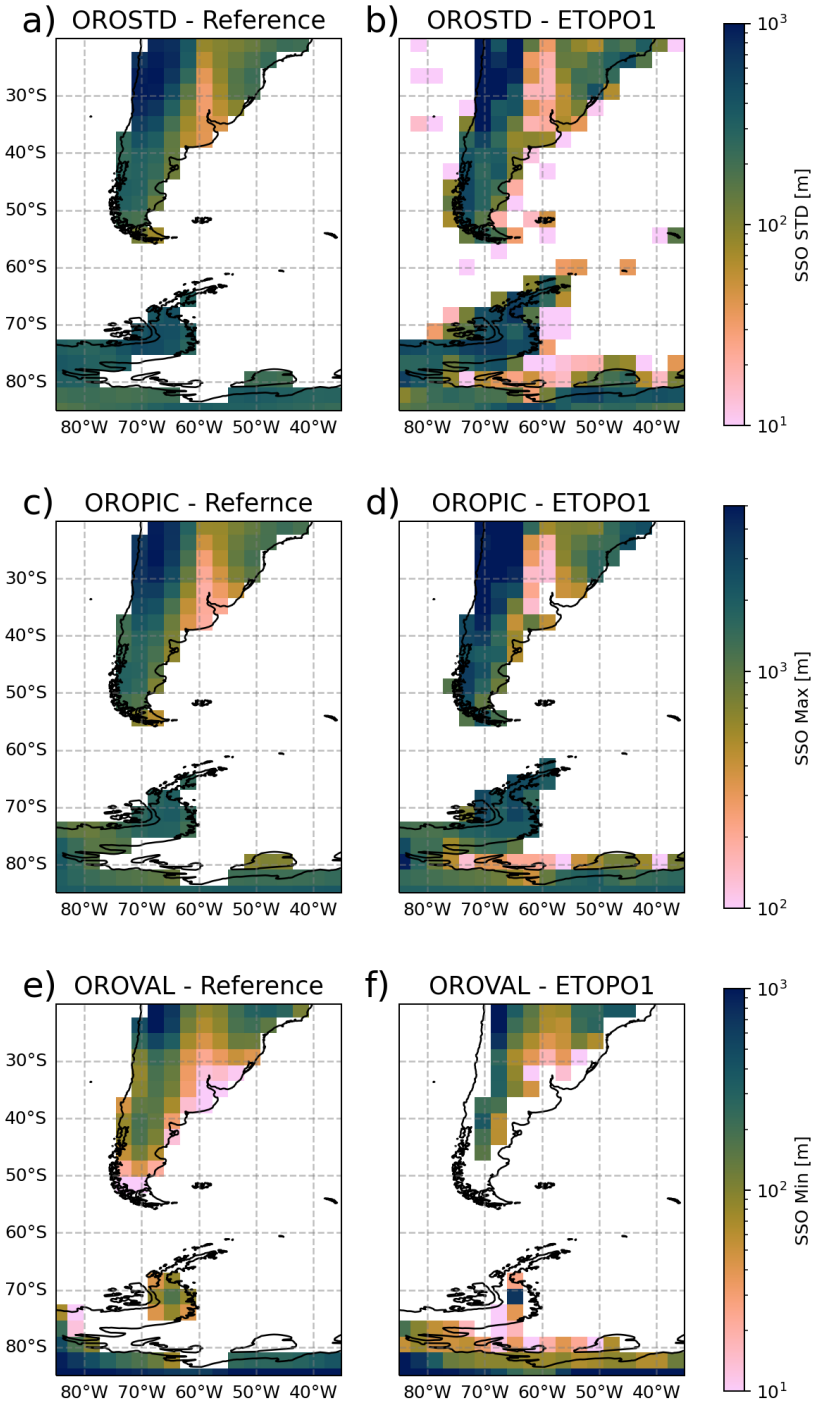

Figure S1. Comparison between subgrid-scale orography parameters a) and b) standard deviation, c) and d) peaks (maxima) and e) and f) valleys (minima) in standard EMAC simulations (left column) and as updated from ETOPO1 high resolution topography data (right column).

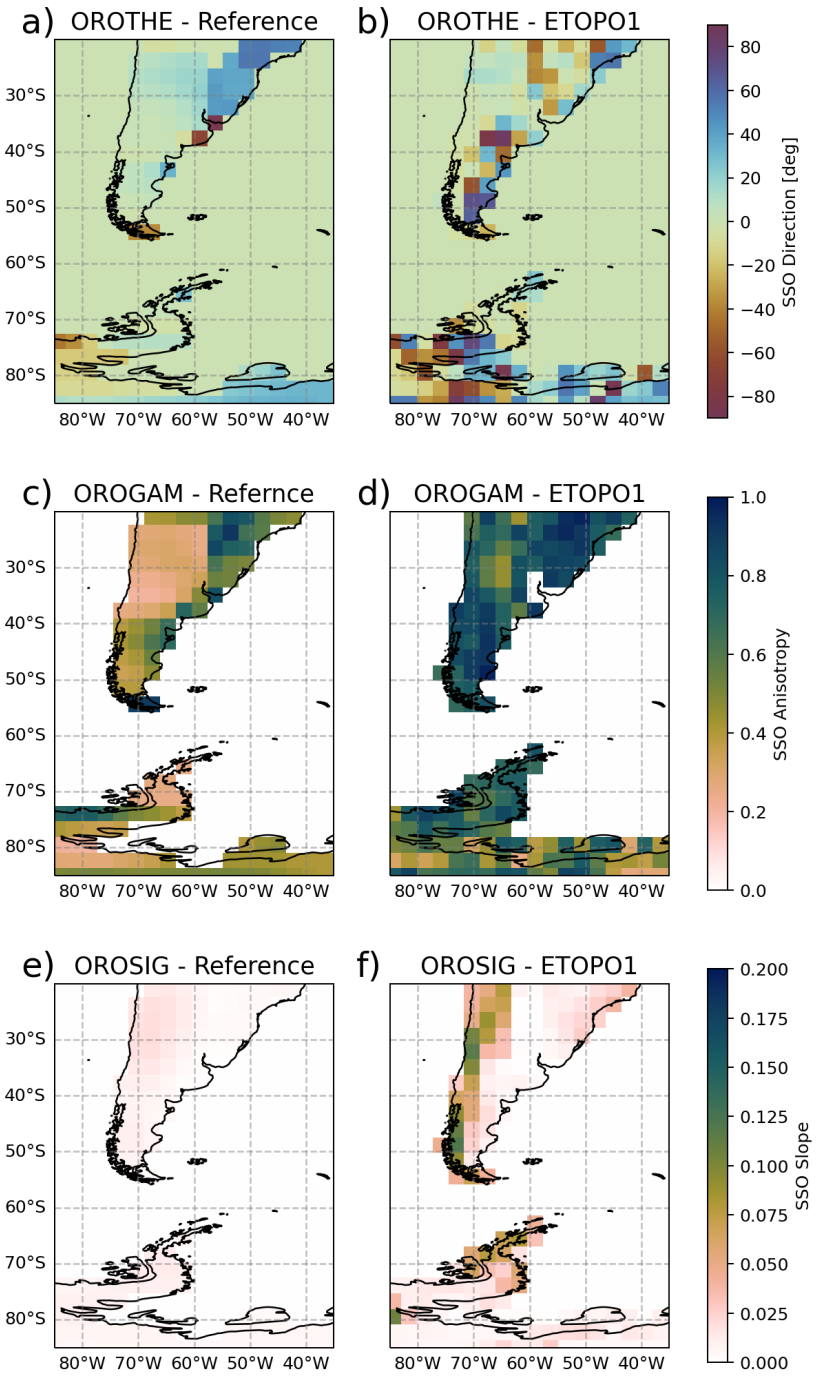

Figure S2. As Fig. S1 but for a) and b) anisotropy, c) and d) slope and e) and f) main orographic angle.

S2 EMAC/MESSy-specific implementation details

In MESSy (Jöckel et al., 2005, 2010), the physical parameterisations themselves are located in the submodel core layer (smcl, messy_orogw.f90 for the orographic GW parameterisation) and the infrastructeure for the physical cores, including the interfaces for coupling the individual modules with the other model parts (including the definition of the channel objects, see Jöckel et al., 2010) are in the submodel interface layer (smil, messy_orogw_si.f90). What is called the physical core in the main text refers to the smcl and the interface is the smil.

Processes that are denoted to be performing at the beginning and at the end of the time step in the main text are implemented in the global_start and global_end routines of the smil, respectively. The global to decomposition (gl2dc) function that is described in Sect 3.1 and in Fig. 5 is the the MESSy-specific function trp_gpdc_gpgl, which is applied to transpose individual fields from one format to another, in our case, from global to decomposition.

In the standard EMAC submodel OROGW, a launch condition check prevents computation of OGW physics in particular columns if the conditions for OGW launching are not fulfilled. This was implemented mainly to reduce computing costs. Now, however, columns that are inactive at the launch site can become active after GW redistribution. Hence, the condition needed to be moved to the computation of the GW flux at Eq. 2 and disabled if the redistribution is activated.

Due to the code design, GW breaking needed to be disabled at the level of redistribution. Consequently, no GW drag can appear at this model level. As GW drag computation in the level of redistribution had to be disabled too (see main text), this has no further consequences.

Fig. S3 shows the hybrid pressure model levels of the EMAC L90MA setup to provide an estimate of the model level altitudes. The top model level is centered around 0.01 hPa

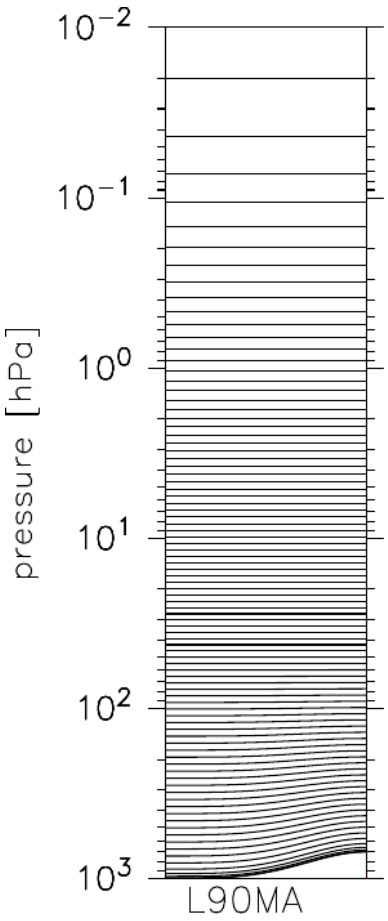

Figure S3. Hybrid pressure levels of vertical resolution L90MA. The terrain-following lower levels near the surface are indicated by an arbitrary elevation shown along the horizontal axis. Figure adapted from Jöckel et al. (2016).

S3 Additional information for the run time performance analysis

The 10 simulations that were carried out for the run time performance analysis of the horizontal redistribution were specifically set using varying numbers of nodes, tasks per node and the associated decomposition. These specifics are shown in Tab. S1. For comparison, each of these setups is applied once with the GW redistribution activated and once without.

Name	Nodes	Tasks/node	PEs	NPXxNPY
perfR/C-1h	1	64	64	8x8
perfR/C-1f	1	128	128	16x8
perfR/C-2f	2	128	256	16x16
perfR/C-4f	4	128	512	32x16
perfR/C-8f	8	128	1024	64x16

Table S1. Overview of the simulations for the computing performance analysis. PEs stands for processing elements, which is the product of nodes and tasks/node. NPXxNPY denotes the global decomposition into latitudinal and longitudinal blocks. Each setup is performed twice, once with GW redistribution (R) and once in the standard columnar approach (C).

S4 Additional figures for Sect. 3.4

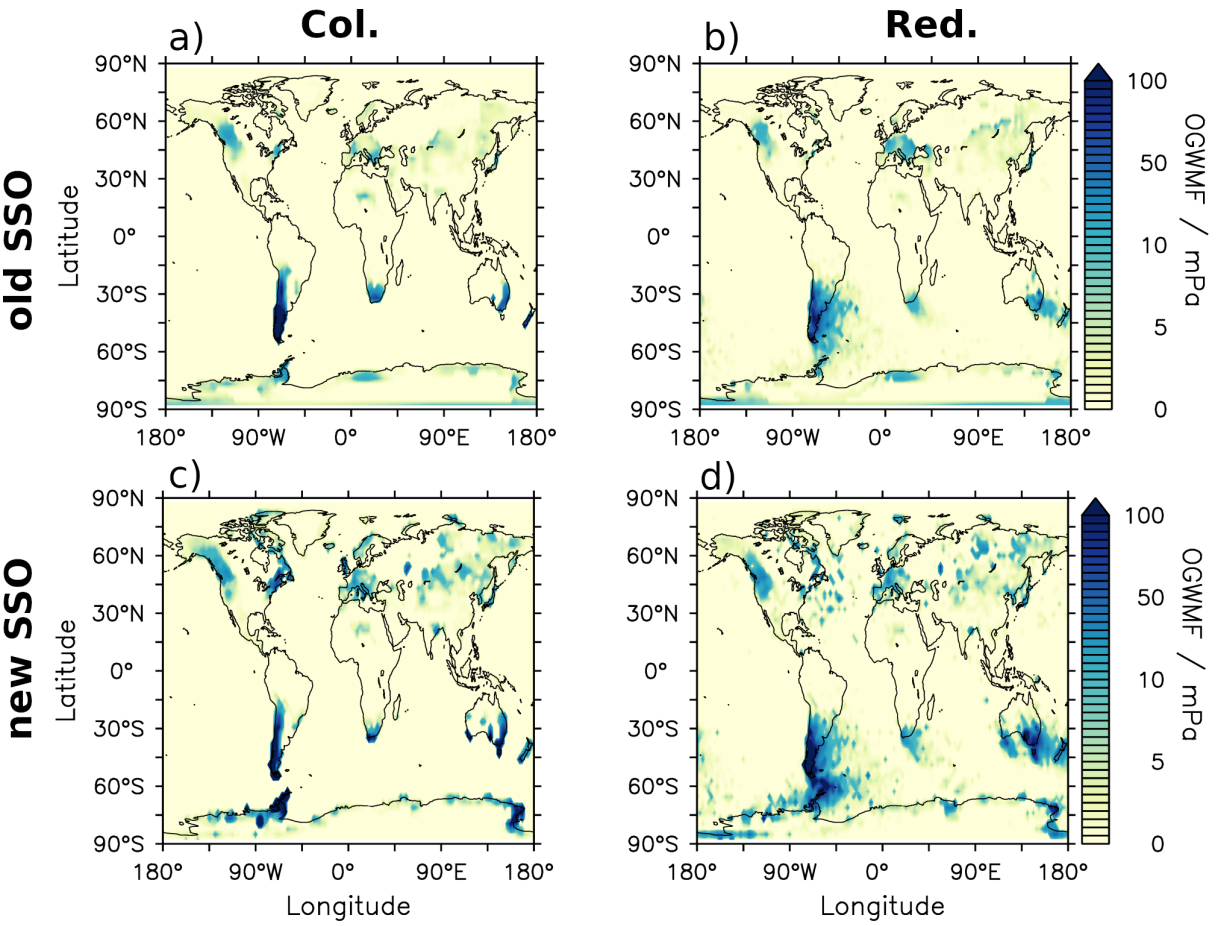

Figure S4. Global monthly mean GWMF at model level 65 for the test simulation month July 2006 for simulations with standard columnar (a and c) GWs and with GW redistribution (b and d) using the old SSO (a and b) and the new SSO (c and d).

S5 Additional figures for Sect. 3.5

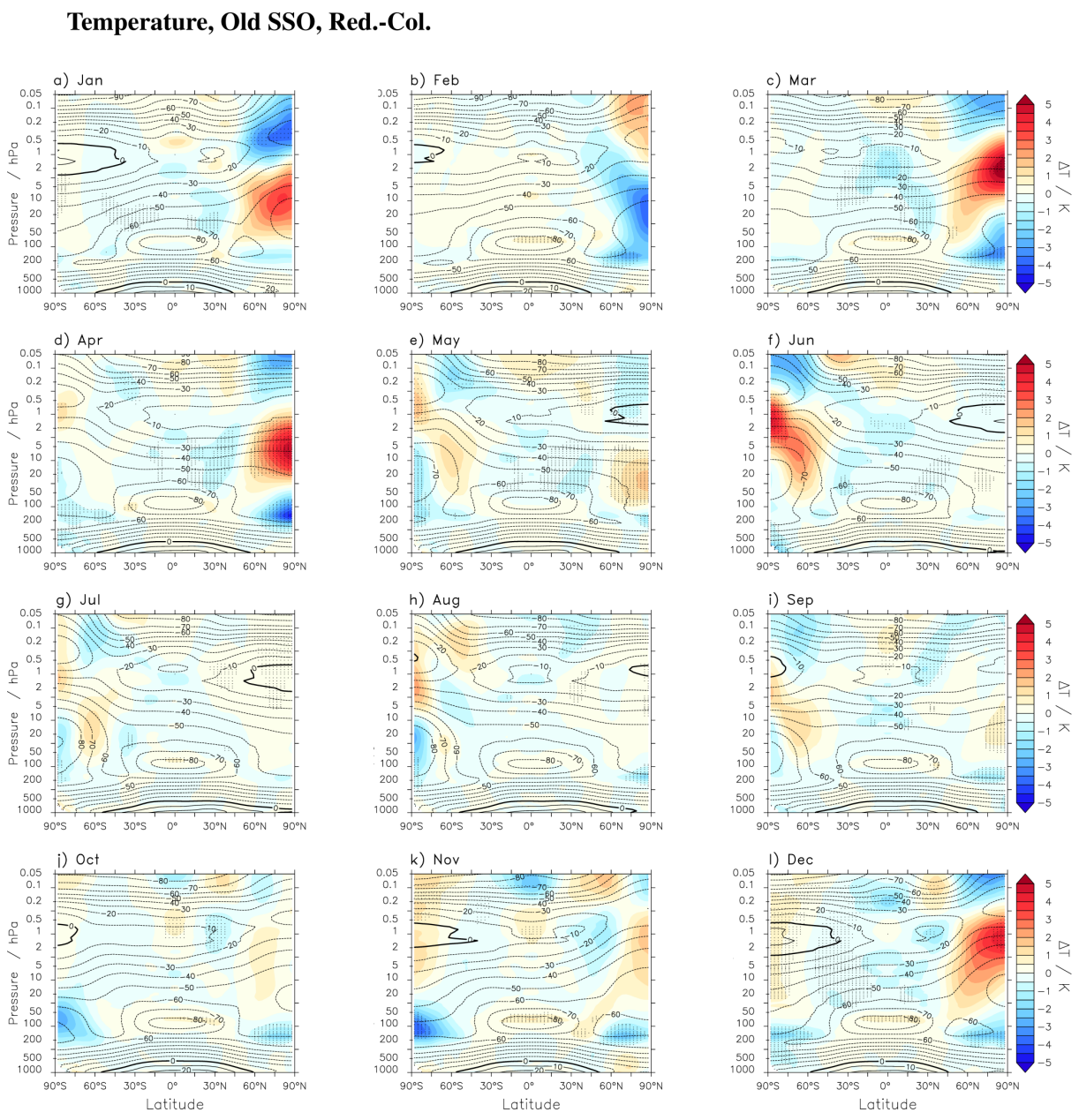

Figure S5. 20 year climatological monthly mean zonal mean temperature differences between the simulations with (Red.) and without (Col. for columnar) OGW redistribution with the old SSO. The contours show the climatologies of the Col. simulation. The dotted regions mark where the differences are significant on the 95% level.

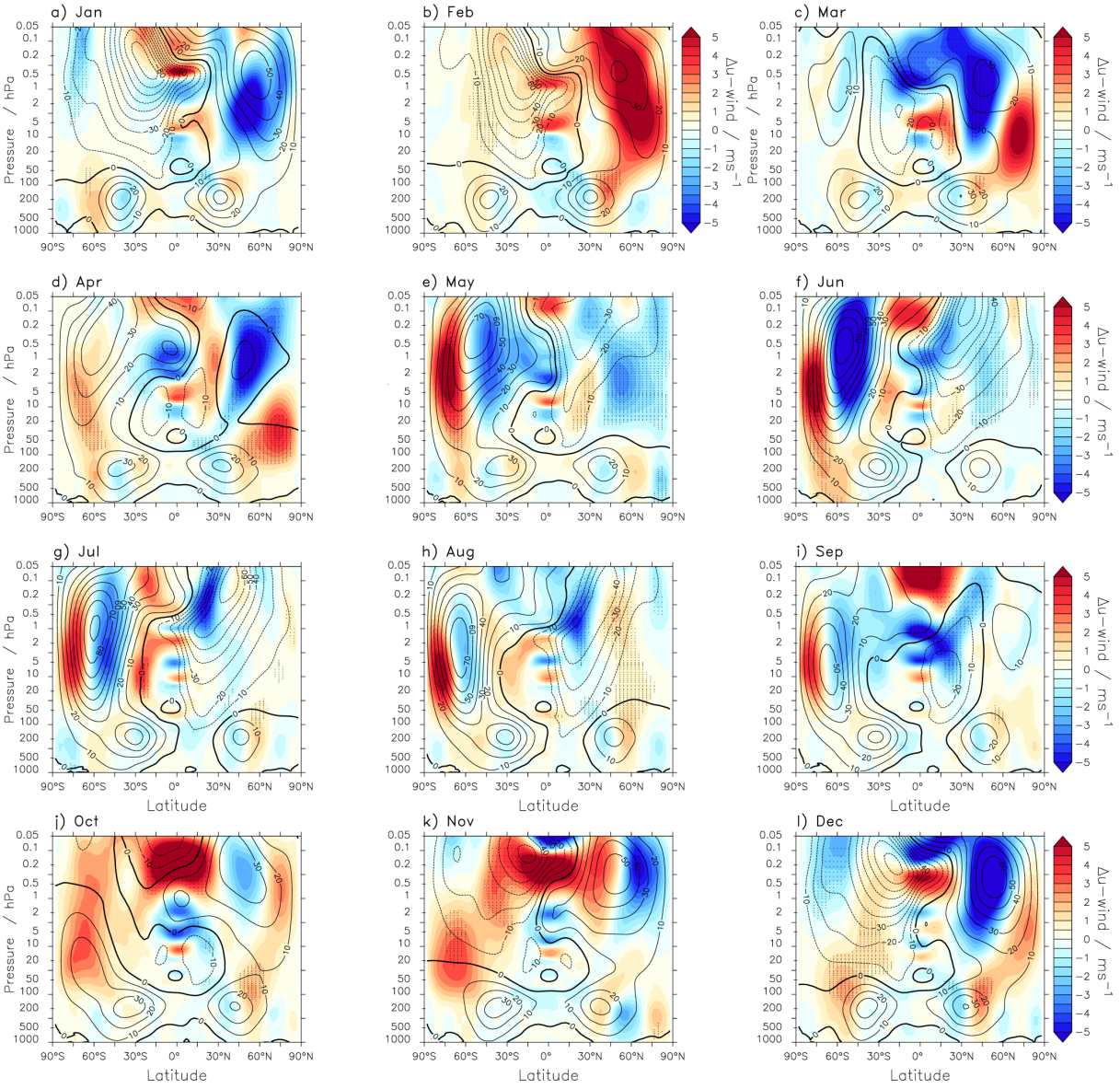

Figure S6. 20 year climatological monthly mean zonal mean zonal wind differences between the simulations with (Red.) and without (Col. for columnar) OGW redistribution with the old SSO. The contours show the climatologies of the Col. simulation. The dotted regions mark where the differences are significant on the 95% level.

Temperature, New SSO, Red.-Col.

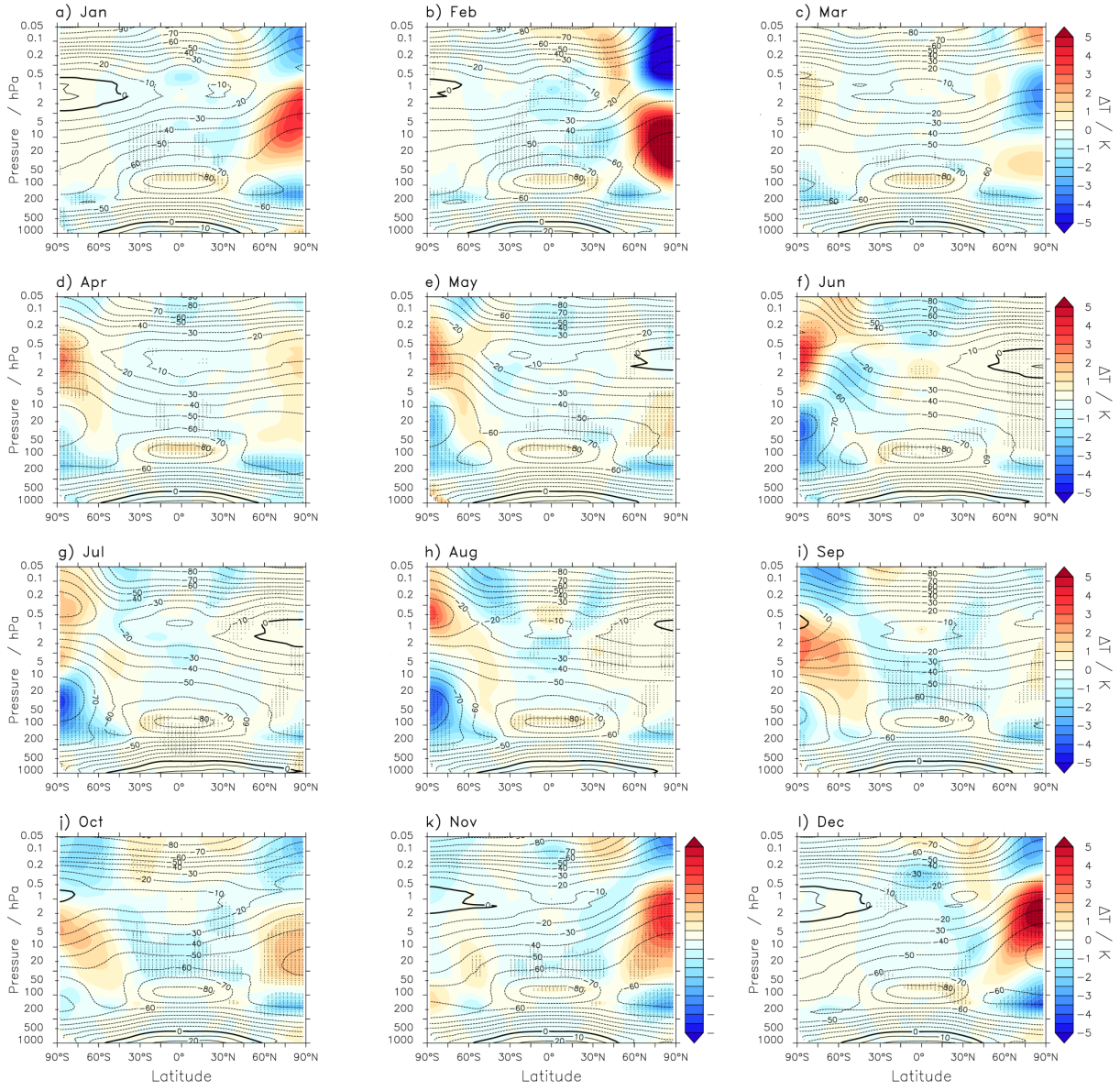

Figure S7. 20 year climatological monthly mean zonal mean temperature differences between the simulations with (Red.) and without (Col. for columnar) OGW redistribution with the new SSO. The contours show the climatologies of the Col. simulation. The dotted regions mark where the differences are significant on the 95% level.

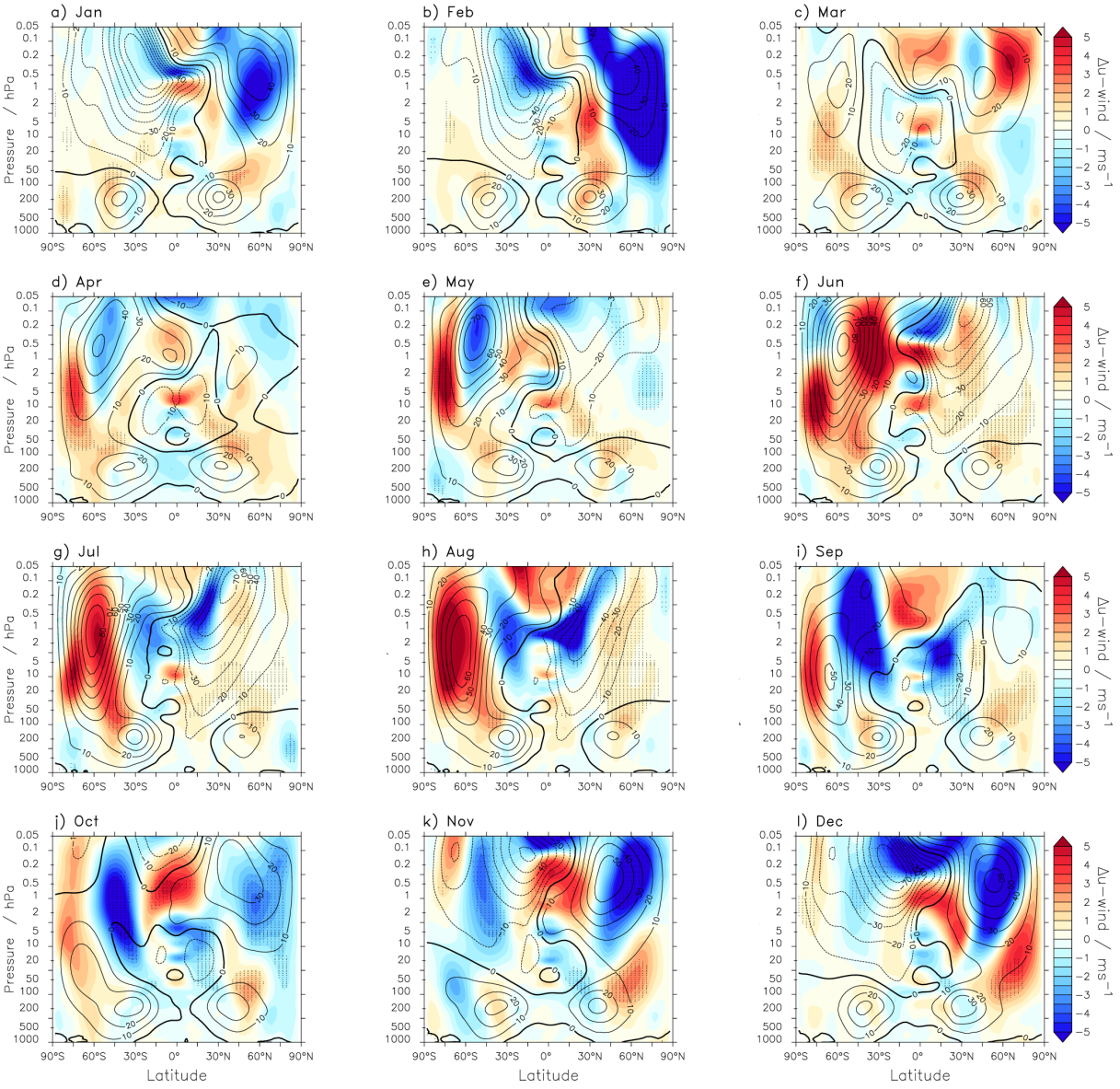

Figure S8. 20 year climatological monthly mean zonal mean zonal wind differences between the simulations with (Red.) and without (Col. for columnar) OGW redistribution with the new SSO. The contours show the climatologies of the Col. simulation. The dotted regions mark where the differences are significant on the 95% level.

Gravity wave drag

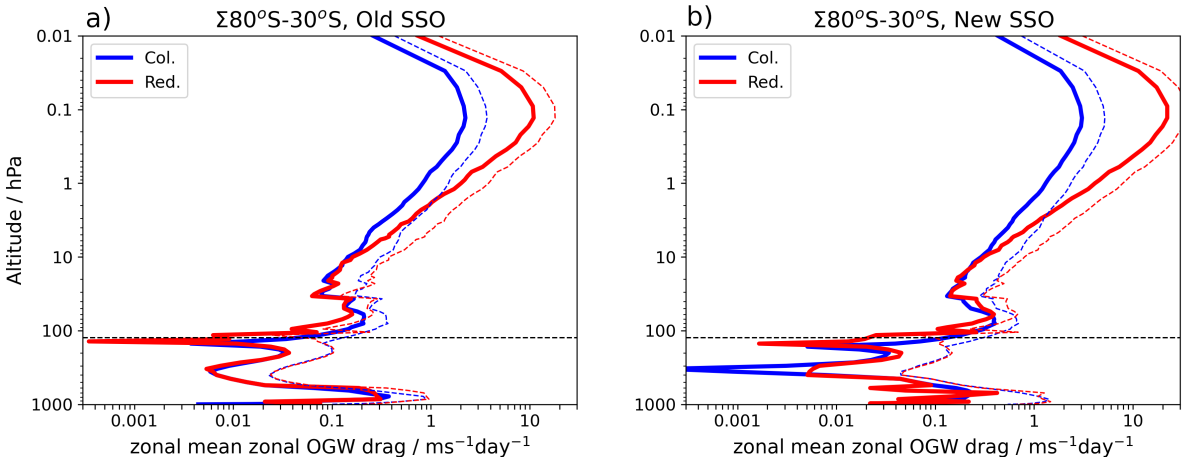

Figure S9. Sum over 80°S-30°S of climatological JJA zonal mean zonal OGW drag of the simulations with (Red.) and without (Col. for columnar) OGW redistribution with a) the old and b) the new SSO. The dashed horizontal line shows the approximate altitude of redistribution (120 hPa). The dashed coloured lines show the 1σ deviation for reference to annual variability. Due to the log depiction, the latter is only possible for one side, as the other side yields negative values.

Geometric polar vortex diagnostics

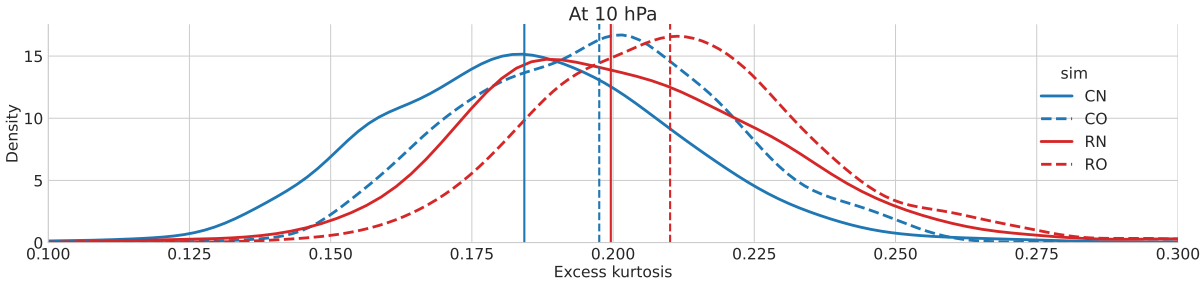

Figure S10. Distribution of Antarctic polar vortex excess kurtosis for JJA at 10 hPa over the 20 simulation years. The different simulations are denoted by C for columnar, R for redistribution, N for new SSO and O for old SSO. The vertical lines depict the median values.

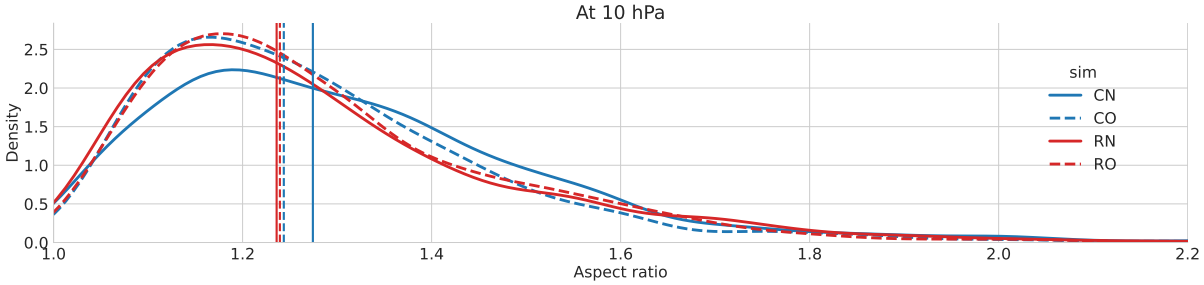

Figure S11. Distribution of the Antarctic polar vortex aspect ratio for JJA at 10 hPa over the 20 simulation years. The different simulations are denoted by C for columnar, R for redistribution, N for new SSO and O for old SSO. The vertical lines depict the median values.

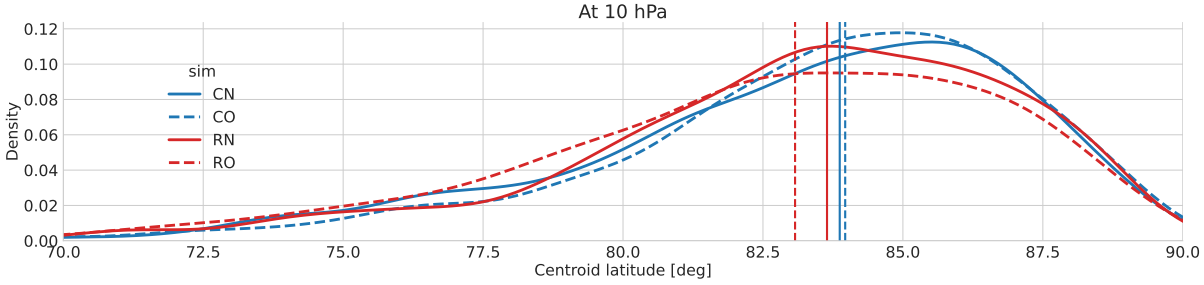

Figure S12. Distribution of Antarctic polar vortex centroid latitude for JJA at 10 hPa over the 20 simulation years. The different simulations are denoted by C for columnar, R for redistribution, N for new SSO and O for old SSO. The vertical lines depict the median values.

References

Amante, C. and Eakins, B.: ETOPO1 1 Arc-Minute Global Relief Model: Procedures, Data Sources and Analysis, https://doi.org/10.7289/V5C8276M, last access: 20 February 2020, 2009.

Baines, P. and Palmer, T.: Rationale for a new physically-based parametrization of subgrid-scale orographic effects, ECMWF Technical Memoranda, pp. 1–11, https://doi.org/10.21957/h4h36b3u, 1990.

Jöckel, P., Sander, R., Kerkweg, A., Tost, H., and Lelieveld, J.: Technical Note: The Modular Earth Submodel System (MESSy) - a new approach towards Earth System Modelling, Atmos. Chem. Phys., **5**, 433–444, https://doi.org/10.5194/acp-5-433-2005, 2005.

Jöckel, P., Kerkweg, A., Pozzer, A., Sander, R., Tost, H., Riede, H., Baumgaertner, A., Gromov, S., and Kern, B.: Development cycle 2 of the Modular Earth Submodel System (MESSy2), Geosci. Model Dev., **3**, 717–752, https://doi.org/10.5194/gmd-3-717-2010, 2010.

Jöckel, P., Holger, T. O., Pozzer, A., Kunze, M., Kirner, O., Brenninkmeijer, C.A, M., Brinkop, S., Cai, D., Dyroff, C., Eckstein, J., Frank, F., Garny, H., Gottschaldt, K.-D., Graf, P., Grewe, V., Kerkweg, A., Kern, B., Matthes, S., Mertens, M., Meul, S., Neumaier, M., Nützel, M., Oberländer-Hayn, S., Ruhnke, R., Runde, T., Sander, R., Scharffe, D., and Zahn, A.: Earth System Chemistry Integrated Modelling (ESCiMO) with the Modular Earth Submodel System (MESSy, version 2.51), Geosci. Model Dev., **9**, 1153–1200, https://doi.org/doi:10.5194/gmd-9-1153-2016, 2016.

Lott, F. and Miller, M. J.: A new subgrid-scale orographic drag parametrization: Its formulation and testing, Quaterly Jounal of the Royal Meteorolocial Society, 123, 101–127, https://doi.org/10.1002/qj.49712353704, 1997.